Sensors and Materials, Vol. 37, No. 3 (2025) 847–860
MYU Tokyo

S & M 3961

Impact of Preferential Flow in Ionic Rare-earth Macropores on Water and Salt Transport by Soil Sensors

Shiliang Zhang,* Xiuzhuang Zhou, and Fengyu Miao

School of Information Engineering, Ningde Normal University, Ningde, Fujian 352100, China

(Received September 30, 2024; accepted February 20, 2025)

Keywords: rare-earth ore, preferential flow, macropores, solute transport, leaching rate

To investigate the impact of preferential flow in ionic rare-earth macropores on water and salt transport, dynamic leaching experiments were conducted on ionic rare-earth ores, with ammonium sulfate as the leaching agent. Indoor column leaching tests were employed to study the transport of the leaching agent in the macropore and matrix zones of soil samples. With the monitoring of the distribution of water potential and solute concentration by soil sensors, the mechanisms of and factors affecting macropore preferential flow were analyzed. Additionally, the relationship between rare earth leaching efficiency and factors such as moisture content, temperature, and solution concentration (electrical conductivity) was examined. To gain a clearer and more intuitive understanding of the water and salt transport process, and to obtain richer data such as the flow velocity distribution for a comprehensive evaluation of various factors affecting macropore preferential flow or solute transport, numerical simulation studies were conducted with Comsol Multiphysics software based on the physical model from indoor experiments. The combined analysis of indoor experiment and numerical simulation results aims to provide technical reference for rare earth leaching in mining operations.

1. Introduction

Owing to the presence of non-interconnected pores in the soil, a soil solution in macropores does not flow when the soil moisture content is low. The solute in this part of the solution only moves by diffusion. The convection dispersion model is a basic model that can reflect the intrinsic mechanism of soil solute transport and is simple in form. However, owing to the spatial variability of soil, this model cannot be used for large-scale solute transport problems in the field. The two-region model, established on the basis of the convection dispersion model, considers the presence of immobile water in the soil and its role in the solute transport process, thereby providing a more accurate description of solute transport in the soil.

Currently, indoor simulation studies on soil macropores and macropore flow at home and abroad mainly use polyvinyl chloride (PVC) soil columns and artificially created macropores for experiments.[1,2] For example, Holden[3] used tension infiltration tests to study the role of soil macropores in runoff production across four types of surface cover and found that only 22% of

*Corresponding author: e-mail: shiliangzh@163.com
https://doi.org/10.18494/SAM5385

ISSN 0914-4935

water flux occurred in pores with a diameter < 0.25 mm. Luo *et al.*[4] studied the impact of soil type and land use on soil macropore characteristics, showing significant effects on soil macroporosity, hydraulic radius, and surface area. Domestically, Sheng *et al.*[5] used different grain sizes of sand and macropore molds to study the 3D transport behavior of macropore flow under ponding conditions. In this study, we showed a high correlation between the transition time of stable wetting fronts and effective surface porosity. Under different effective surface porosity conditions, cumulative infiltration conformed to the Kostiakov model, and macropore connectivity dominated preferential infiltration under certain conditions. Xu and Cheng[6] conducted preferential flow infiltration tests on the basis of large soil columns, revealing that differences in loess infiltration mainly stem from soil pore structure and connectivity rather than total pore volume, indicating that loess macropores are the main channels for preferential rainfall infiltration, with macropore connectivity affected by rainfall amount and temperature conditions. Sheng and Fang[7] used a large macropore formed in the center of a soil column made of organic glass to simulate solute breakthrough under preferential flow conditions. Studies have shown that soil macropores significantly affect water transport owing to the highly nonequilibrium nature of macropore flow and its regional characteristics.

Although the indoor artificial simulation of macropore preferential flow experiments has achieved certain results, these studies[8–11] mainly focus on the impact of rainfall infiltration on preferential flow, observing and analyzing the relationship between wetting fronts, infiltration volume, infiltration rate, and preferential flow development, or using indicators such as stained area ratio to quantitatively analyze preferential flow. However, there is little research on the distribution of soil water potential and solute, analyzing the mechanisms of and factors affecting macropore preferential flow, and studying the relationships among solution concentration, moisture content, temperature, and electrical conductivity. Whether the distribution cloud map of leaching rate can reflect the solution flow situation and whether a relationship can be established between the development degree of macropores and solution flow are of significant theoretical and practical value for studying the impact of macroporosity development on the leaching rate of rare-earth ores. The study is aimed at determining the hydraulic intrinsic connection between macropore flow and matrix flow and the impact of soil macropore water salt movement on rare earth leaching rate using a combination of indoor experiments and model simulations.

2. Materials and Methods

A two-region model simulating macropore flow was established.[12,13] Since water movement in the matrix zone adheres to Darcy's Law, the Richards equation with pressure as the dependent variable is used for calculations. For macropores, the capillary force can be neglected, and the kinematic wave equation is adopted. For solute transport in the matrix domain, the model uses the convection dispersion equation. For the macropore domain, where the flow velocity is relatively high and solute transport is mainly by convection, the dispersion effect can be ignored, and the convection equation is directly used to calculate the solute transport in the macropore domain.

The infiltration equations for water flow in the macropore and matrix domains, with water head as the variable, are represented with the subscripts *f* for the macropore domain and *m* for the matrix domain, as shown in Eqs. (1) and (2).

$$C_f \frac{\partial h_f}{\partial t} = \frac{\partial}{\partial z}(K_f \frac{\partial h_f}{\partial z} + K_f) - \frac{\lambda_w}{w_f} \tag{1}$$

$$C_m \frac{\partial h_m}{\partial t} = \frac{\partial}{\partial z}(K_m \frac{\partial h_m}{\partial z} + K_m) + \frac{\lambda_w}{1 - w_f} \tag{2}$$

Here, t represents the time variable s; w_f denotes the volume ratio of the macropore domain to the entire soil body; h denotes the pressure head m; K is the unsaturated hydraulic conductivity in m/s; θ is the water content in cm^3/cm^3; λ_w represents the water exchange term between the two domains in 1/s; C is the water capacity in 1/L.

In the dual-permeability model, the most critical is the coupling term between the two domains. The relationship between the water exchange term and the pressure head between the two domains in the dual permeability model can be represented by Eq. (3).

$$\lambda_w = \alpha_w (h_f - m_f) \tag{3}$$

Here, α_w represents the first-order water exchange coefficient, which is specifically expressed as

$$\alpha_w = \frac{\beta}{d^2} r_w K_{sa} . \tag{4}$$

Here, β is the soil aggregate geometric shape factor, which takes the values of 3 for a rectangular prism and 15 for a sphere; d is the distance from the center of the aggregate to the boundary of the macropore (in cm); r_w is the empirical parameter, taken as 0.4; K_{sa} is the hydraulic conductivity coefficient at the interface between the two domains, which is determined as

$$K_{sa} = 0.5(K_m(h_f) + K_m(h_m)) . \tag{5}$$

The dual permeability model describes both the macropore and matrix domains using the Richards equation, which is solved using the implicit finite difference method. A certain depth of soil is taken, and the calculation region is divided into N elements, with a total of $N + 1$ nodes, where $N = 0$ and $N = i$ are the boundary nodes. An equal distance step size is used, and the Richards equation is discretized in time and space according to the implicit difference scheme. For the solute parts,

$$\frac{\partial \theta_f c_f}{\partial t} + \frac{\partial f \rho s_f}{\partial t} = \frac{\partial}{\partial z}(\theta_f D_f \frac{\partial c_f}{\partial z}) - \frac{\partial q c_f}{\partial z} - \varphi_f - \frac{\Gamma_s}{w} , \tag{6}$$

$$\frac{\partial \theta_m c_m}{\partial t} + \frac{\partial (1-f)\rho s_m}{\partial t} = \frac{\partial}{\partial z}(\theta_m D_m \frac{\partial c_m}{\partial z}) - \frac{\partial q c_m}{\partial z} - \varphi_m - \frac{\Gamma_s}{1-w}. \tag{7}$$

Here, w denotes the volume fraction of the fracture network in all pores, $w = \theta_{fs}/\theta_s$, the other variables being the same as before.

For the porous medium, the dilute substance transfer solute transport (convection, texture transfer of the porous medium, and dispersion) implements the coupling of solute transport with Darcy flow.

$$\frac{\partial(\varepsilon_p c_j)}{\partial t} + \frac{\partial(\rho c_{p,j})}{\partial t} + \nabla \cdot J_j + u \cdot \nabla c_j = R_j + S_j \tag{8}$$

Here, $J_j = g(D_{F,j} + D_{e,j})\nabla c_j$, $\theta = \varepsilon_p$, $D_{e,j} = \frac{\varepsilon_p}{\tau_{F,j}} D_{F,j}$, $\tau_{F,j} = \varepsilon_n^{-1/3}$.

In the Comsol Multiphysics software, we add the module for the transfer of dilute substances in porous media, which includes the unsaturated porous medium model (incorporating dispersion and adsorption models), the reaction module, and related computational modules. Additionally, we define and implement a generalized partial differential equation with relevant material properties for simulation and solution. Within the reaction module, a chemical reaction kinetics model is constructed by considering the exchange interactions between the cations of the leaching agent and the rare-earth ions.

$$(\theta_i + \rho_b k_{pi})\frac{\partial c_i}{\partial t} + c_i \frac{\partial \theta_i}{\partial t} + u_i \cdot \nabla c_i + \nabla \cdot (-\theta_i D_{Li} \nabla c_i) = \theta \phi_{Li} c_i + \rho_b k_{pi} \phi_{pi} c_i + S_c \tag{9}$$

$$\begin{aligned} \theta D_{Lii} &= \alpha_1 \frac{u_i^2}{|u|} + \alpha_2 \frac{u_j^2}{|u|} + \theta \frac{D_m}{\tau_L} \\ \theta D_{Lij} &= \theta D_{Lji} = (\alpha_1 - \alpha_2)\frac{u_i u_j}{|u|} \end{aligned} \tag{10}$$

Here, i is $\{f, m\}$; ϕ_L denotes the decay rate of the dissolved solute concentration, with units of 1/d; ϕ_p signifies the decay rate of the adsorbed solute concentration, also with units of 1/d; the hydrodynamic dispersion tensor D_L represents the mechanical dispersion apart from chemical diffusion; τ_L is a tortuosity factor, $\tau_L = \theta^{-7/3}\theta_s^2$; and all the other parameters are the same as previously mentioned.

The reaction control equation utilizes the Gapon equation, which is an ion exchange equation derived on the basis of kinetic principles and is similar to the Kerr equation.[14] Experimental results indicate that when the ionic composition of the exchange phase changes, the range of variation in the selectivity coefficient obtained through the Gapon equation is relatively small.[15] Currently, the Gapon equation has been widely applied in the study of soil exchange reactions, and it exhibits the smallest range of variation in ion exchange selectivity coefficient with changes in ion concentration compared with others.

3. Experiments

The soil samples used in this experiment were collected from a rare earth mine in Pingnan, Fujian. Particle analysis and density measurements were conducted on the samples. The analysis revealed that the soil sample has a density of 2.54 g/cm³, a porosity of 47%, a residual moisture content of 2.5%, and a saturated hydraulic conductivity *K*s of $2.943 \times 10^{-6} - 2.943 \times 10^{-6}$ m/s. The particle size distribution indicated that the soil sample is salty clay loam. Saturated hydraulic conductivity is a crucial parameter for soil water movement, reflecting the infiltration and percolation properties of the soil. Estimating the hydraulic conductivity using soil transfer functions is time-saving and labor-efficient. Therefore, we employ the software methods of Residual Energy Transfer Curve (RETC) and Soil Water Characteristic Curve (SWC) to calculate the saturated hydraulic conductivity of both the matrix and macropore domains of the soil. By inputting the content of silt, sand, and clay particles, along with the bulk density into the interface, the parameters of the SWC empirical equation and the saturated hydraulic conductivity can be obtained, as shown in Fig. 1. In the SWC subroutine, by entering the content of silt and clay particles, preliminary values of the soil's saturated hydraulic conductivity, wilting point, field capacity, saturated moisture content, as well as the SWC and unsaturated hydraulic conductivity curve, can be obtained.

The experimental apparatus shown in Fig. 2 consists of a cuboid column with dimensions of 100 cm length, 30 cm width, and 85 cm height. During the experiment, a 2-cm-thick layer of fine sand was first spread at the bottom to ensure that the outflow was not blocked. Then, a 60-cm-high layer of test soil was filled into the column. An outlet was installed at the bottom of the soil column to collect the outflow. A partially automatic liquid collector was used every 1.5 h

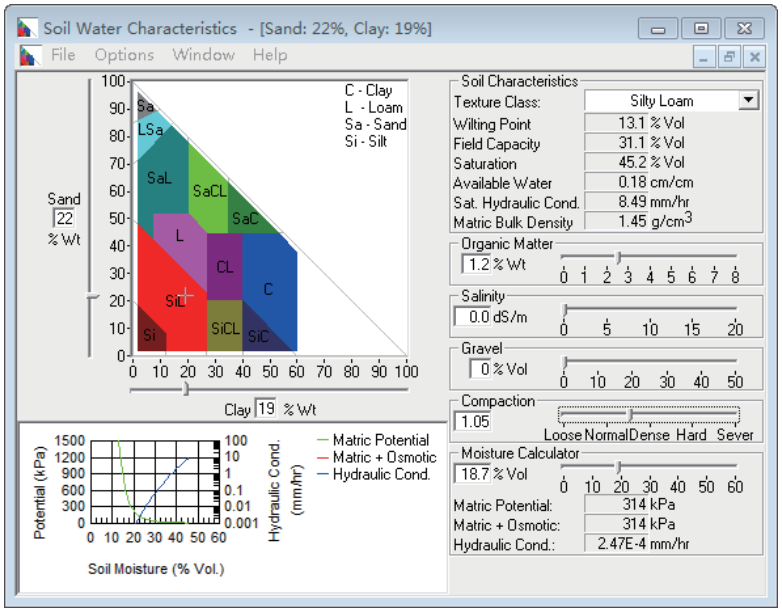

Fig. 1. (Color online) Estimation of saturated hydraulic conductivity by SPWA program.

to collect the outflow for monitoring the rare earth concentration at different times. Additionally, a drainage outlet was located at the top of the right side to maintain a constant water head of 5 cm during liquid injection. After filling the soil, a filter paper was placed at the top of the soil column to prevent the topsoil from being washed away during water injection. A peristaltic pump was used to inject a 2% ammonium sulfate solution at a controlled rate. When the outflow rare earth concentration reached 0.03 g/L, the solution was replaced with water until the outflow concentration dropped to 0.01 g/L, at which point the injection was stopped. When an electric current passes through an electrolyte solution, ions move directionally, allowing for conductivity. The electrical conductivity of the soil solution is closely related to the ion concentration and charge in the solution, as well as the ion migration rate. There is a linear relationship between ion concentration and electrical conductivity in the solution. By measuring electrical conductivity, the ion concentration in the soil solution can be indirectly determined. To obtain the soil sample's moisture content, temperature, and ion concentration at different times, three multifunctional soil sensors were embedded at corresponding positions on both sides of the soil column. The soil moisture sensors, composed of stainless steel probes and waterproof heads, can be buried in the soil for long-term use, enabling the online monitoring of temperature, moisture content, and electrical conductivity in both surface and deep soil samples. These sensors can measure relative humidity, temperature, and electrical conductivity, with values of 100%, 100 °C, and 20000 μS/cm, respectively. Two sensors were used to measure the macropore area (sensors 4 and 6), while

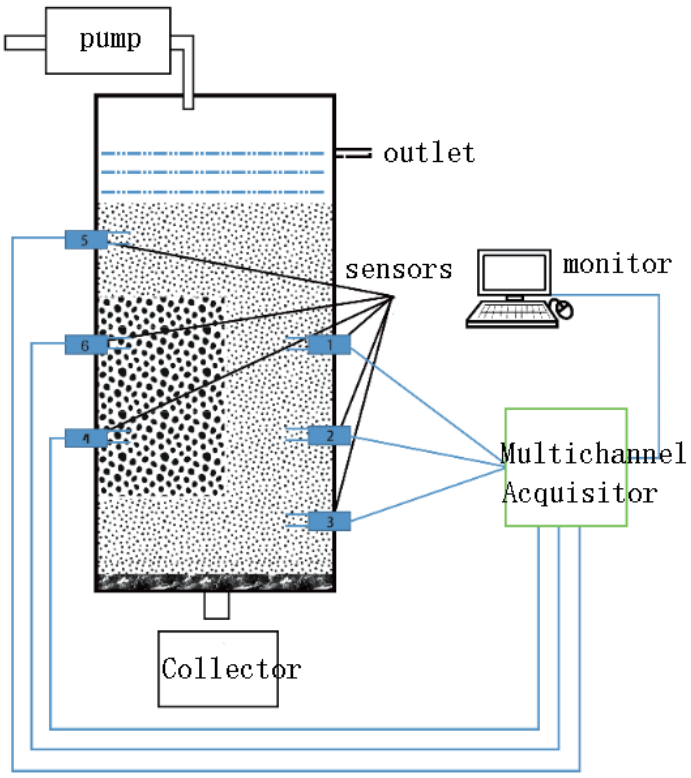

Fig. 2. (Color online) Column immersion experimental device.

the remaining four sensors measured the matrix area. A multichannel collector was used to gather data from the sensors, with a data collection interval set to 5 min. Continuous data on temperature, humidity, and electrical conductivity were collected.

4. Results and Discussion

4.1 Rare-earth ion concentration breakthrough curve

The concentration of rare-earth ions in the leachate was determined using the EDTA titration method. When the concentration of rare-earth ions in the leachate was less than 0.01 g/L and the injection was stopped, a graph was plotted with the total outflow mass (g) on the horizontal axis and the leachate rare-earth ion concentration (g/L) on the vertical axis, as shown in Fig. 3.

Figure 3 shows that the concentration of leached rare earth forms a bimodal pattern. The first peak appears when the leachate is around 3500 g, and the second peak appears near 6500 g. The rare-earth ion concentration initially increases rapidly, reaching a peak, and then decreases. The rate of decrease is lower than the rate of increase. The bimodal pattern may be due to the left and right sides of the soil column belonging to the matrix and preferential flow zones, respectively. In the initial stage, the macropores are filled with air and there is no water flow, so the hydraulic conductivity of the macropores can be neglected, and the matrix conducts most of the water flow, which moves relatively slowly. When the water potential of the soil sample reaches the infiltration pressure of the macropores, water flow begins to occur in the macropores. After 14 days, the soil sample's water content continues to increase, reaching or approaching saturation. The macropores, which are strongly connected in the vertical direction, will fully conduct water and be governed by gravity. Water flows rapidly in the macropores, and the soil sample's hydraulic conductivity increases exponentially. The ability of the macropores to conduct water will far exceed that of the matrix zone, leading to a significant nonequilibrium flow state in the soil sample. The early initial breakthrough, tailing, bimodal phenomenon, and asymmetry of the breakthrough curve, as well as the increased water movement rate in the soil sample due to preferential flow, and the earlier appearance of the peak concentration of the leachate, all strongly indicate the impact of preferential flow in the macropores.

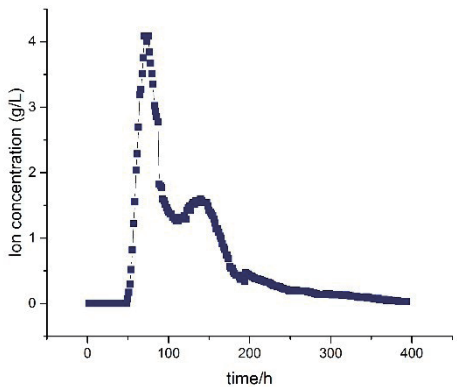

Fig. 3. (Color online) Concentration breakthrough curve of rare-earth mother liquor.

4.2 Analysis of rare earth moisture content changes

When the column leaching began, the initial mass moisture content of the soil sample was 18.73%. As shown in Fig. 4, after the column leaching started, the overall trend of changes in moisture content recorded by the sensors did not differ significantly. The peak value appeared after the injection of clean water. The curve first increased, then fluctuated and rose to the maximum value, and then quickly dropped to the minimum value. The sensor readings varied at different positions. Overall, as the depth increased, the moisture content decreased, and the moisture content in the matrix zone was greater than that in the macropore preferential flow zone. During the rising phase, sensors 1, 2, and 5 showed the largest fluctuations and increases, whereas sensors 3, 4, and 6 showed slower fluctuations and increases, reaching a maximum of around 62%. Sensor 4 showed relatively minimal changes. The fastest changes during the rising phase were observed in sensors 1 and 5, which are located in the upper matrix zone of the soil column. They showed rapid increases for about a day, followed by slower increases, and then started to decrease after 14 days. By February 25, the moisture content recorded by different sensors began to drop sharply at different times, and by March 5, all sensors had reached the lowest value of around 24%. Generally, the curves that rose quickly also dropped quickly, with some delay between different curves. Sensors 1 and 5 are located in the matrix zone, where the pores are small and evenly distributed, resulting in high matrix suction and rapid increases in moisture content. In the macropore region, owing to larger pores and lower matrix suction, the initial increase in moisture content was slower. This is because the surface layer of the soil column had not reached or was close to saturation, preventing macropore flow. As the surface moisture content increased, larger macropores began to conduct water quickly. During the injection period, the matrix zone, with its evenly distributed pores, absorbed more water. In contrast, in the preferential flow zone characterized by significant macropore structures, the hydraulic conductivity changes sharply with increasing moisture content when nearing saturation. This explains why the moisture content is lower and more variable in sensors 4 and 6 than in the matrix zone. Another possible reason is that not all macropores extend throughout the entire soil profile. The internal water collection area formed in a macropore that is closed at one

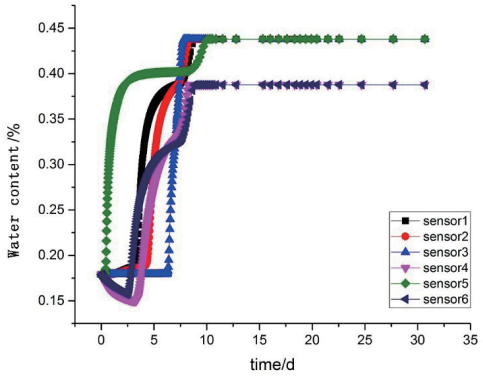

Fig. 4. (Color online) Relationship between water content and time.

end is also known as a dead-end macropore, which can affect the distribution of soil moisture content.

After the start of column leaching, lateral water exchange occurs between the water flow in the macropores and the matrix. As the moisture content in the macropores increases, the water flow speed increases. When the vertical water flow rate in the macropores is much greater than the lateral water exchange rate, there is not enough time for the moisture content and solute concentration to reach equilibrium with the slowly moving water retained in the soil matrix. This results in significant nonequilibrium flow, causing the curves to be fluctuating rather than smooth. After the injection ends, the more macropores there are in the soil sample, the faster the moisture loss from the soil matrix. The more macropores present in the soil sample, the lower the overall moisture content. After the injection stops, the rate of moisture loss from the soil matrix increases with the number of macropores. Without a source of water replenishment, the water in the soil matrix will move downward and be expelled from the soil sample under gravity, and this portion of water will flow out through the bottom hole. Soil samples with higher moisture content will have faster water movement in the soil matrix, while those with lower moisture content will have slower water movement in the soil matrix.

4.3 Analysis of ion concentration changes in soil samples during leaching

On the basis of data collected from multifunctional soil sensors distributed at different positions, the changes in ion concentration during the rising and falling phases of the ore body were studied. A time interval of 5 min was used as the unit for the horizontal axis, and the ion concentration was plotted on the vertical axis, as shown in Fig. 5.

From Fig. 2, we can see that the ion concentration changes in the ore body at various sensor locations are abrupt, with fluctuations ranging between the maximum value and 50 μs/cm. The largest jumps were observed in sensors 4 and 6, which are located in the preferential flow zone. Since the maximum range of sensor conductivity is only 200 μs/cm, the maximum value is 200 μs/cm. The time taken for these jumps varies. Sensors buried in the matrix zone (sensors 1, 2, 3, and 5) reached their peak values in a relatively short time. Although sensor 1 is buried deeper than sensor 5, the moisture content in sensor 1 reached its peak earlier. This is because the soil layer above sensor 1 is entirely in the matrix zone, with small pore diameters and high capillary suction. Initially, smaller pores absorb water more easily, and the leachate is more readily absorbed. When the surface soil sample approaches saturation, the macropore preferential flow zone begins to conduct water and becomes the main channel for water movement, causing significant nonequilibrium flow and solute migration.

Additionally, during the actual infiltration process, the surface layer of the soil sample rarely reaches full saturation in a short time. Not all highly connected macropores are directly supplied with water from the surface. There are many isolated “dead pores” in the soil sample, and only a few macropores can reach saturation. Under unsaturated conditions, thin layer flow or rivulet flow may occur on the walls of the macropores. Therefore, the concentration fluctuations in the artificial preferential flow zone are high, and the duration of the jumping fluctuations is longer.

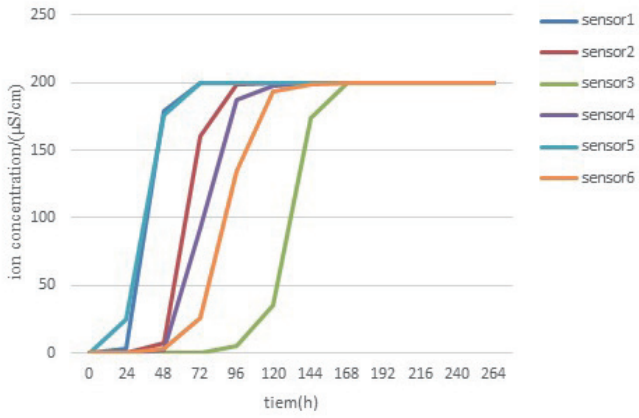

Fig. 5. (Color online) Ion concentration curves at different sensors during injection.

Another potential reason is that not all macropores extend throughout the entire soil profile depth, displacing relatively high rare-earth ions, which thins the double electric layer on the clay soil profile. This increases the attraction between particles and tends to cause aggregation, increasing the clay porosity and clay pore diameter. Moreover, as the moisture content of the clay increases, large amounts of soluble salts dissolve in the pore water, significantly increasing the ion concentration of the solution. When weak acid salts such as soluble carbonates dissolve in the pore water, these ions may undergo chemical reactions to produce insoluble salt precipitates, blocking the pores, and reducing the of the clay porosity, and clay pore diameter.

From Fig. 5, it can be seen that during the drainage phase after the injection stops, the ion concentration at each sensor location decreases very quickly. Within approximately 2 days, the concentration at each sensor drops to its lowest value. Sensors 1 and 5 show the fastest decrease, whereas sensors 4 and 6 show the slowest decrease, accompanied by fluctuations. This indicates that the ion concentration decreases quickly in non-macropore areas but decreases more slowly in the artificial macropore preferential flow zone. The slowest decrease is observed in the lower preferential flow zone, which is even slower than in the bottom matrix zone. When the ion concentration in other areas reaches its minimum value, the lower preferential flow zone still has a value of 24 μs/cm. The slow change may be due to the fact that when the macropores drain, water from the matrix slowly discharges into the macropores. Additionally, there may be some dead-end pores in the macropores, retaining a significant portion of the solution.

4.4 Analysis of the relationship between various parameters during leaching

From the curves of moisture content and ion concentration in the ore body, it can be observed that the increase in moisture content is relatively slow, with an intermediate plateau phase, reaching its maximum value after approximately 16 days. In contrast, the ion concentration rises rapidly, reaching its peak value (2000 μs/cm) within one day. As the moisture content of the clay gradually increases, soluble salts continuously dissolve in the pore water, raising the ion

concentration of the soil sample. Between the 23rd and 27th days, the moisture content remains at its maximum value, while the ion concentration begins to decrease on the 25th day, with some sensors showing the lowest values by the 28th day. This indicates that during the rising phase, the trends of moisture content and ion concentration are consistent, whereas during the falling phase, the trends are opposite. Next, we analyze the relationship between the mother liquor concentration and the ion concentration in the ore body. The maximum concentration of the leachate occurs on the fourth day (February 11) and the sixth day (February 13), corresponding to the time when the ion concentration in the soil sample reaches its peak. This suggests that the higher the ion concentration in the soil sample, the better the leaching effect. However, as the amount of rare earths being leached decreases, even if the ion concentration in the ore body remains constant, the amount of rare earths that leached out gradually decreases, leading to the tailing phenomenon in the mother liquor breakthrough curve.

5. Comparative Study of Simulation Experiments

Since the soil column experiment could not monitor the distribution of flow velocities in the seepage zone, and the monitoring points for moisture content and ion concentration were limited, it could not fully reflect the spatiotemporal distribution of water potential and solutes in the seepage zone. Therefore, we conducted numerical simulations on the basis of the physical model of the column leaching experiment. By combining the column leaching experiment and numerical simulations, we comprehensively analyzed the rules and factors affecting the water-soluble solute transport under macropore preferential flow. The column leaching was simulated using multiple Richards equations combined with the transport of dilute substances in porous media, ignoring the effect of air. The Richards equation is given by

$$\begin{aligned} &\frac{\partial(\varepsilon_p \rho)}{\partial t} + \nabla \cdot (\rho u) = Q_m, \\ &u = \frac{k}{\mu}(\nabla p + \rho g). \end{aligned} \tag{11}$$

The formula for dilute substance transfer in porous media is

$$\begin{aligned} &\frac{\partial(\varepsilon_p c_i)}{\partial t} + \frac{\partial(\rho c_{p,j})}{\partial t} + \nabla \cdot J_i + u \cdot \nabla c_j = R_i + S_i, \\ &J_i = -(D_{D,j} + D_{e,j}) \nabla c_j. \end{aligned} \tag{12}$$

Here, pressure p is the dependent variable, C_m represents the specific moisture capacity, S_e denotes the effective saturation, S stands for the storage coefficient, K_s indicates the hydraulic conductivity, μ represents the fluid dynamic viscosity, k_r denotes the relative permeability, ρ represents the fluid density, g stands for the gravitational acceleration, D represents elevation, and Q_m represents the fluid source (positive) or sink (negative).

Using COMSOL Multiphysics for simulation work, we set the parameters such as porosity and dispersion to be consistent with the conditions of the indoor experiments. The initial conditions of the model were set according to the conditions of the indoor experiments. The initial conditions for pressure head were set to be consistent with the conditions of the indoor experiments, and the initial solute concentration was set to zero. When solving the basic equation of soil water movement and the convection dispersion equation, the finite difference method was used. The time step and iteration information were set to default values, and then adjusted on the basis of simulation results to reduce numerical noise. The appropriate mesh size was adjusted to improve the simulation efficiency and accuracy. The Darcy velocity was coupled with solute transport, and the distribution results of Darcy velocity after six days in the soil column are shown in Fig. 6; we can see that after six days, initially, due to the matrix suction effect, the water flow velocity was much greater in the matrix than in the macropore region. As infiltration continued, the ore body gradually reached saturation, and water flow moved under the effect of gravity. The flow velocity was much higher in the preferential flow zone than in the matrix. Both velocities increased initially and then stabilized at a certain speed. The water flow velocity was higher in the preferential flow zone than in the matrix, and the solute concentration continuously increased. Initially, the solute in the matrix moved quickly under negative pressure with a high concentration. After about one day, the concentration in the macropore region rose rapidly, faster than in the matrix. As time passed, the solute concentration continued to rise, and eventually, when both regions reached saturation, their concentrations were essentially equal.

The exchange rate of substances between the two domains is not only related to the transport depth of macropore flow but also to the degree of imbalance in moisture content and solute concentration between the two domains. In the initial stage of infiltration, the exchange rate of water and solutes between the two domains is higher in the surface soil sample than in the lower layers. However, after a period of time, the exchange rate in the surface layer gradually decreases. This is because the moisture content and solute concentration in the matrix domain of the upper soil sample continuously increase. As they approach the matrix's saturation moisture content, the degree of imbalance between the two domains becomes less pronounced, leading to a pause in substance exchange. Overall, the dual domain model can reflect the nonequilibrium nature of water and salt transport in soil samples with macropores.

6. Conclusions

Despite the potential for pore blockage due to fine particle migration, concentration differences, and clay mineral expansion and dissolution during the leaching of ion-adsorption rare-earth ores, this study's artificial macropore regions are filled with coarse sand, making the impact of fine particle migration negligible. As the leaching agent percolates, migrates, and transforms within the rare-earth ore, complex physical, chemical, and biological reactions occur, altering the unsaturated characteristics and microstructure of the ore. Water flow in the matrix and macropores undergoes lateral exchange, with significant nonequilibrium flow occurring only when the vertical flow rate in the macropores considerably exceeds the lateral exchange

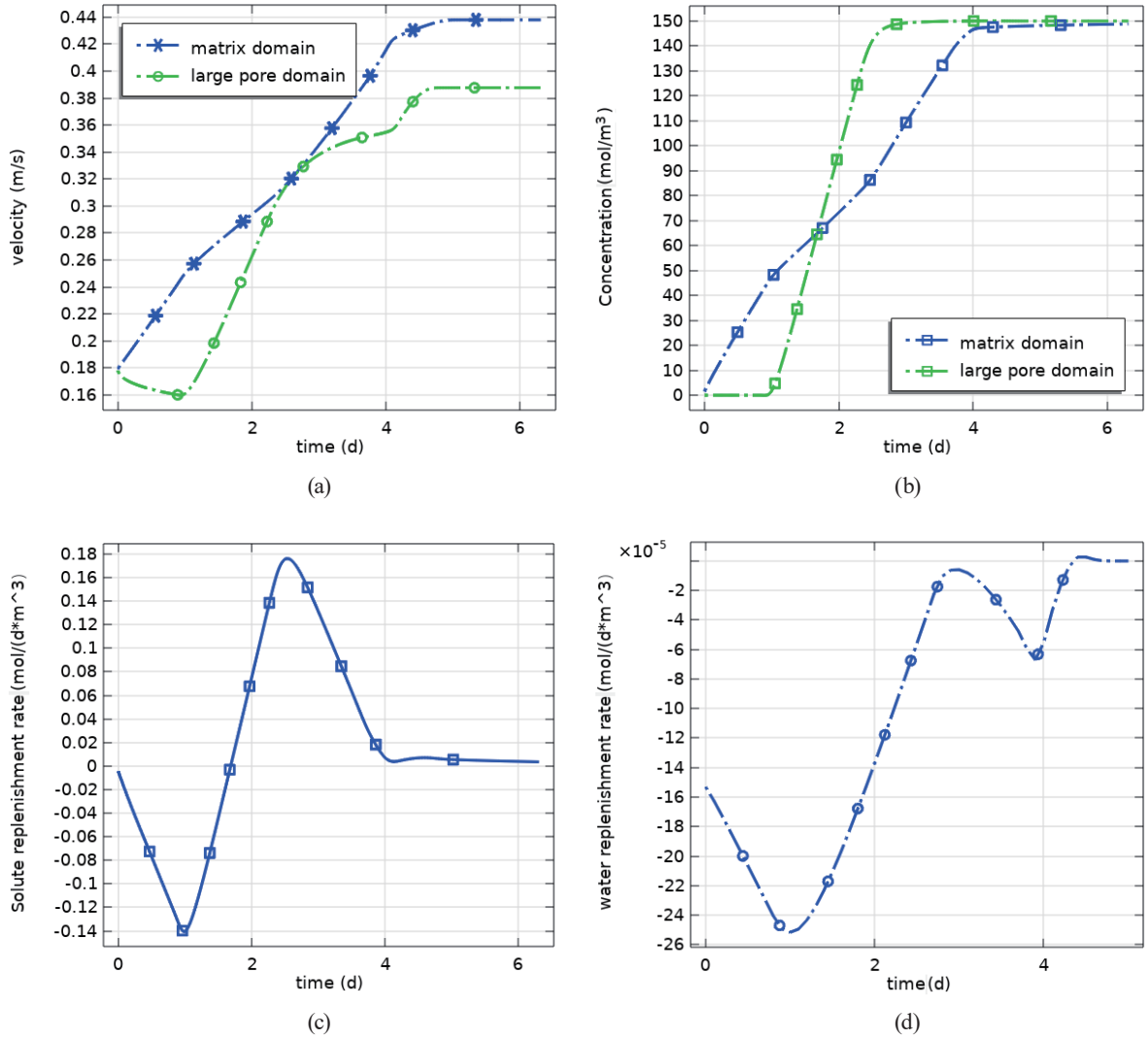

Fig. 6. (Color online) Solute exchange between two domains: (a) variation curve of Darcy velocity, (b) variation curve of solute concentration, (c) water exchange, and (d) solution exchange.

rate. The substance exchange rate between the two domains is related to the migration depth of the macropore flow and the imbalance in water content and solute concentration. The results obtained from monitoring with multifunctional soil sensors and numerical simulations conducted in physical models are consistent, thereby validating the reliability of the indoor simulation experiments.

(1) In summary, the seepage, transport, and transformation of the leaching agent in the rare-earth layer not only undergo changes from unsaturated to saturated moisture states but also involve complex physical, chemical, and biological reactions. These processes further induce changes in the unsaturated characteristics and microstructure of rare earths. The interactions between water, salt, and rare-earths exhibit different characteristics and patterns at different transport times and depths.

(2) When the negative pressure head in the soil sample exceeds the infiltration pressure, macropore flow is generated. This phenomenon is related to the initial moisture content of the soil sample, the duration of column leaching, the amount and intensity of the injected liquid, and the saturated hydraulic conductivity of the soil matrix. Changes in water supply, air pressure, and pore structure can also result in intermittent pulse flow. Therefore, the concentration fluctuation range in artificial preferential flow zones is macropore, with prolonged and more pronounced jumps, leading to a bimodal shape in the leachate concentration curve.

(3) Comparing the results monitored by multifunctional soil sensors with the numerical simulation results of transport in the physical model, we found that both methods yield consistent results. Both can determine the speed and direction of water and salt transport, indicating that the indoor simulation experiment has a certain degree of reliability. Its conclusions and analytical process provide preliminary guidance for field applications.

Acknowledgments

This work was supported by the Natural Science Foundation of Fujian of China (grant number 2023J011090) and the Ningde Normal University Special Funding Program Research Project (grant number 2023ZX416). The authors would like to thank the editors and reviewers for their valuable comments and suggestions.

References

1 Y. W. Ni, Z. Q. Qu, and P. Ying: J. Appl. Ecol. **12** (2001) 103. https://pubmed.ncbi.nlm.nih.gov/11813410/
2 X. Li, Y. Lu, X. Zhang, W. Fan, Y. Lu, and W. Pan: Environ. Geol. **78** (2019) 1. https://doi.org/10.1007/s12665-019-8527-2
3 J. Holden: J. Hydrol. **364** (2009) 342. https://doi.org/10.1016/j.jhydrol.2008.11.010
4 L. Luo, H. Lin, and S. Li: J. Hydrol. **393** (2010) 53. https://doi.org/10.1016/j.jhydrol.2010.03.031
5 F. Sheng, H. Liu, K. Wang, R. Zhang, and Z. Tang: J. Hydrol. **508** (2014) 137. https://doi.org/10.1016/j.jhydrol.2013.10.048
6 X. X. Xu and T. L. Cheng: J. Soil Water Conserv. **4** (2010) 4. https://d.wanfangdata.com.cn/periodical/trqsystbcxb201004018
7 F. Sheng and Y. Fang: Soils **44** (2012) 144. https://www.oalib.com/paper/1420810
8 Y. Liang, R. F. Xia, T. J. Yeh, Z. W. Sun, H. J. Zhang, and B. Xu: Eng. Geol. **340** (2024) 119. https://doi.org/10.1016/j.enggeo.2024.107692
9 L. Luo and H. Lin: Vadose Zone J. **8** (2009) 233. https://doi.org/10.2136/vzj2008.0010
10 E. Casali, M. Larsbo, J. Koestel, and N. Jarvis: J. Hydrol. **630** (2024) 341. https://doi.org/10.1016/j.jhydrol.2024.130732
11 J. Wu, J. Zhang, and R. Gao: Agric. Eng. **23** (2009) 35. https://doi.org/10.3969/j.issn.1002-6819.2009.10.003
12 H. H. Gerke and G. M. Van: Water Resour. **29** (1993) 305. https://doi.org/10.1029/92WR02339
13 S. Zhang and X.. Liu: Microelectron. Reliab. **93** (2019) 115. https://doi.org/10.1016/j.microrel.2019.01.009
14 W. S. Pan, Y. F. Xu, Y. D. Lu, L. Gao, X. Yao: Trans. Chin. Soc. Agric. Eng. **33** (2017) 140. https://doi.org/10.11975/j.issn.1002-6819.2017.03.019
15 S. Zhang, X. Liu, and G. Sun. Sens. Mater. **33** (2021) 1989. https://doi.org/10.18494/SAM.2021.3279